ADVANCED FUNCTIONAL MATERIALS
www.afm-journal.de

Modified Highly Elastic 3D Nanofiber Embolic Scaffolds for Precise In Situ Embolization Therapy

Pengfei Cai, Lei Cao, Yangfan Ding, Yu Han, Xiao Yu, Jie Cui, Hongsheng Wang, Jinglei Wu, Mohamed EL-Newehy, Meera Moydeen Abdulhameed, Xiumei Mo, Shoubao Wang,* and Binbin Sun**

Transcatheter arterial embolization (TAE) is an effective treatment for hemangiomas or highly vascular tumors. However, conventional embolic agents have limitations such as off-target embolization, regurgitation, and embolic migration, which can affect the efficacy and safety of embolic therapy. The study designed a highly elastic modified embolic scaffold constructed with Polycaprolactone/Gelatin (PCL/GEL) nanofibers to achieve precise in situ embolization in vivo. The embolic scaffolds can be extruded to a small size for smooth intervention in the vessel and rapidly regain their volume when reaching the target area. The results of the in vitro study indicate that the embolic scaffolds modified with lysine and PEI exhibit good biocompatibility and functionality. Furthermore, the in vivo rabbit ear embolization test demonstrated that the modified embolic scaffolds fit closely to the vessels and induced a significant amount of neo tissue deposition in the embolized area. The embolization process using the modified embolic scaffolds is safe and stable and results in more desirable embolization outcomes compared to commercial gelatin embolic agents. In conclusion, the modified highly elastic embolic scaffolds designed in this study offer a novel method for in situ embolization that has potential for clinical application in TAE.

1. Introduction

In recent decades, transcatheter arterial embolization has been considered an effective treatment for aneurysms,[1] hypervascular tumors,[2] and traumatic hemorrhage with low invasiveness and high clinical efficacy. The embolic substances used in transcatheter arterial embolization are referred to as embolic agents, and traditional solid embolic agents include gelatin sponge particles,[3] polyvinyl alcohol particles,[4] and coil springs.[5] However, there are still shortcomings with commercial embolic agents, such as a high risk of off-target embolization with granular embolic agents[3] and a risk of hemangioma exposure with coil springs due to low to 15% occlusion rates.[6] These potential risks can cause ischemia and serious complications in normal tissues or lead to reduced embolization efficacy or even treatment failure.[7] Therefore, how to achieve precise embolization and ensure the embolization effect is the key to solving the above problems.

Recently, many researchers have developed novel embolic agents to improve the efficiency and success of embolization.[8–10] Novel in situ gel hydrogel embolization agent, which can inject fluidized hydrogel into the embolization target area through catheter intervention and adjust the properties of the hydrogel through physical and chemical factors to achieve in situ gel

P. Cai, Y. Ding, X. Yu, J. Cui, H. Wang, J. Wu, X. Mo, B. Sun
State Key Laboratory for Modification of Chemical Fibers and Polymer Materials
Shanghai Engineering Research Center of Nano-Biomaterials and Regenerative Medicine
College of Biological Science and Medical Engineering
Donghua University
Shanghai 201620, China
E-mail: xmm@dhu.edu.cn; binbin.sun@dhu.edu.cn

L. Cao
Orthopaedic Traumatology, Trauma Center, Shanghai General Hospital, School of Medicine
Shanghai Jiao Tong University
Shanghai 201620, China

Y. Han
Department of Orthopaedics
The First Affiliated Hospital of Zhengzhou University
Zhengzhou 450052, China

M. EL-Newehy, M. M. Abdulhameed
Department of Chemistry
College of Science
King Saud University
P.O. Box 2455, Riyadh 11451, Saudi Arabia

S. Wang
Department of Plastic and Reconstructive Surgery, Shanghai Ninth People's Hospital
Shanghai Jiao Tong University School of Medicine
Shanghai 200011, China
E-mail: 120021@sh9hospital.org.cn

The ORCID identification number(s) for the author(s) of this article can be found under https://doi.org/10.1002/adfm.202316590

DOI: 10.1002/adfm.202316590

formation, thus achieving precise embolization.[2,11,12] The key to the performance of in situ gel hydrogel embolization agents is to control and balance the critical gelation time to achieve precise in situ gelation in the embolization region.[13] However, it is difficult to balance the smoothness of hydrogel material delivery in the catheter and the in situ gelation performance in the target area.[14] In clinical, how to accurately achieve their gelation in the embolization region is where the difficulty lies, because hydrogel materials are susceptible to a variety of factors such as temperature and stress. In addition, uncontrolled degradation of hydrogel materials may lead to intravascular movement of hydrogel fragments, resulting in ectopic embolization or embolization failure.[13] Therefore, it is of utmost importance to develop new embolic agents that combine precise targeting and efficient embolization.

For the application needs of the new embolic agents, we propose to develop an embolic scaffold that meets the following key requirements. i) Appropriate mechanical properties with good elasticity and shape recovery. Before embolization, it allows the embolic scaffold to be extruded to a small size for microcatheter delivery and to rapidly regain its volume for precise embolization within the vessel lumen, thus avoiding embolization off-target problems. ii) Good procoagulant ability. In embolization, it can effectively improve the success rate of embolization and achieve efficient embolization. iii) Good biocompatibility for cell/tissue grow-in. After embolization, it permits embolic scaffolds to have substantial cellular infiltration and neo tissue deposition after implantation, resulting in more complete embolization of the target area.

Electrospinning, which is widely used in biomedical applications to process biomaterials to produce nanofibrous scaffolds mimicking the extracellular matrix.[15] Generally, the electrospun nanofibrous scaffolds are 2D structures with low porosity, which is not conducive to cell infiltration. Thus, many studies have focused on the preparation and application of 3D nanofibrous scaffolds by electrospinning.[16–18] Xie et al.[19] constructed a gelatin nanofibrous elastic sponge dressing with electrospun 3D nanofibrous scaffold, which exhibited excellent liquid-absorbing ability, good mechanical properties, and good hemostatic effect for bleeding. Wang et al.[20] constructed a highly flexible 3D scaffold using silica nanofibers. The elastic fiber scaffold can be used in minimally invasive surgery, unfolding after implantation to fit the defect site perfectly and promote bone regeneration. Overall, the 3D scaffolds which are constructed from electrospun nanofibers typically have a microscopic fibrous structure and controlled mechanical properties. Based on this, we believe that 3D nanofiber-based embolic agents can be prepared by electrospun nanofibers with good compressible and elastic mechanical properties. In addition, the 3D nanofiber scaffolds constructed from various types of biomaterials can be further modified, providing the possibility of biofunctional modification of the embolic agents. Therefore, we believe that solid embolic agents prepared by nanofiber 3D scaffolds may have a unique advantage in embolization therapy. In addition, there are no studies and reports related to 3D nanofiber scaffolds designed for embolization therapy.

Gelatin (GEL) is a product of multi-step hydrolysis of collagen, with low irritant response to tissue contact.[21] It has good hemostatic properties and has been widely used for commercial purposes such as wound healing and embolization agents.[22–24] Polyethyleneimine (PEI) is a branched or linear cationic polymer with a strong and stable positive surface charge.[25] Its abundant amine moiety gives it the advantage of high functionality and thus has a wide range of applications in nanomedicine. The procoagulant effect of PEI has been investigated and its coagulation mechanism has been clearly elucidated.[26] It has been shown that PEI can induce platelet aggregation and platelet activation and has demonstrated good hemostatic effects.

Therefore, in this study, we constructed an embolic scaffold with high elasticity using Polycaprolactone/Gelatin (PCL/GEL) nanofibers and improved its functionality using PEI modification. The ratio of PCL to GEL was confirmed, and the component with the most suitable mechanical properties and shape recovery ability was selected by mechanical property testing. The embolic scaffold was then tested for cytocompatibility and hemocompatibility to assess its safety. The procoagulant and antimicrobial abilities of the embolic scaffolds were tested to assess their biofunctionality. Finally, in vivo testing was performed using a rabbit ear embolization model to histologically assess the ability of the embolic scaffolds to achieve precise in situ and efficient in vivo embolization.

2. Results

The preparation process of the highly elastic modified embolic scaffold was shown in **Scheme 1**. First, PCL/GEL nanofiber membrane was prepared by electrospinning. Then, the nanofiber membrane was homogenized at high speed to obtain dispersion nanofibers. The uncrosslinked scaffold was obtained by casting and molding of the dispersion nanofibers, and then followed by lyophilization. Finally, followed by treating with glutaraldehyde solution, the crosslinked scaffolds was obtained with high elastic mechanisms. The highly elastic embolic scaffolds (crosslinked scaffolds) were then modified with amino group from PEI, and lysine, respectively. On the one hand, the modified embolic scaffolds grafted with PEI solution contains a large amount of free amino groups, which may play a role in promoting coagulation. On the other hand, the modified embolic scaffolds were treated with lysine to eliminate the toxic effects of the remaining aldehyde residues on the cells. Finally, the modified highly elastic embolic scaffolds were obtained.

To obtain embolic scaffolds with sufficient mechanical properties and high coagulation capacity, the GEL and PCL materials were mixed in different ratios to determine the optimal composition (**Figure 1A**). Based on the previous experience,[27] five PCL/GEL nanofiber membranes with different ratios were prepared in this study. SEM results showed that all of the PCL/GEL nanofiber membranes had smooth surfaces and uniform distribution of nanofiber diameters, and the diameters of the nanofibers in each group were close (Figure 1B,E). The nanofibers were converted into short nanofibers using a high-speed homogenizer, which had a looser structure (Figure 1C). The short nanofibers were then crosslinked to form a 3D structure scaffold by glutaraldehyde treatment, and the crosslinking caused the scaffold to shrink (Figure 1A). Significantly, during the high-speed homogenization process, it was observed that the challenge of homogenizing nanofibers increased progressively with the rise in the PCL component. It was attributed to the high flexibility of the PCL material, which proves resistant to breakage.

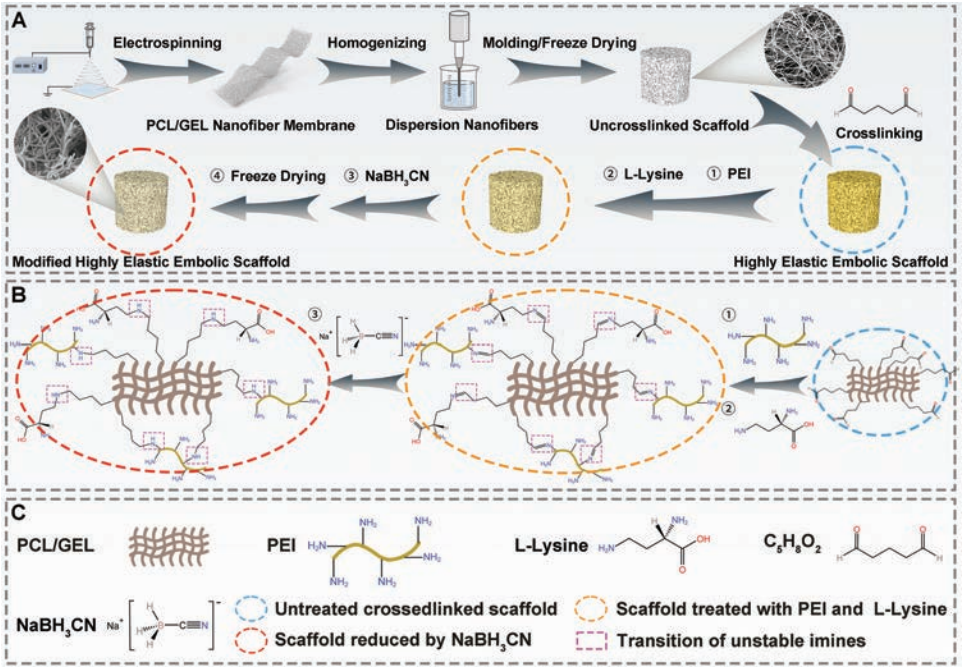

Scheme 1. A) Schematic illustration of the fabrication process for the modified highly elastic embolic scaffold. B) Chemical bonding process during modification. C) Illustration of each type of substance in the modification process.

SEM results revealed that scaffolds with higher PCL contents exhibited localized agglomeration and uneven dispersion after the crosslinking process (Figure 1D). This also leaded to macroscopic collapse of the scaffolds (Figure 1A).

The mechanical properties of highly elastic embolic scaffolds with various components were assessed via mechanical testing. **Figure** 2A demonstrates the stress–strain curves for each scaffold group in a wet state. All scaffolds followed Hooke's law during the first compression phase and maintained their structural integrity up to 80% of the strain range. Both the compressive modulus and the maximum compressive stress of the scaffolds showed an increase with the rise in PCL content, as shown in Figure 2B,C. Among the groups studied, the P-G/5-95 scaffold displayed the lowest compressive modulus of 12. 07 ± 1.21 kPa while the P-G/10-90, P-G/15-85, and P-G/20-80 scaffolds had compressive moduli of 18.75 ± 1.71 kPa, 19.87 ± 1.83 kPa, and 21.81 ± 1.63 kPa, respectively. Meanwhile, the P-G/25-75 scaffold exhibited the highest compressive modulus of 36.96 ± 3.92 kPa. Compression cycle tests were performed on each group, as shown in Figure 2D–H. In 100 compression cycles at a strain rate of 60%, no significant loss of maximum stress was observed, but recoveries varied widely (Figure 2I). The scaffolds showed excellent fatigue resistance with little permanent deformation after 60% compression when the ratio of PCL to GEL was <10% (Figure 2D,E,J). On the other hand, the scaffold demonstrated poor fatigue properties with a ratio of PCL greater than or equal to 15%. The compression cycle curve reveals that the scaffold exhibited ≈30% permanent deformation as denoted by the horizontal line area in the red line box (Figure 2F–H,J). This deformation occurred due to the uneven distribution of nanofibers caused by high PCL content in the material. For meeting the in vivo implantation conditions for embolic scaffolds, the P-G/10-90 group (known as the PG group) was preferred because of its superior fatigue resistance and higher compressive modulus in comparison to the P-G/5-95 group.

The PG group's scaffolds were modified with chemical modifications. Lysine was used as a foundation material to generate PGL scaffolds, increasing their biocompatibility. In addition, PEI was employed to produce PGPL-L and PGPL-H scaffolds, with the goal of boosting their procoagulant characteristics, respectively. The four scaffold groups were identified as follows: PG (without modification), PGL (with lysine modification), PGPL-L (with lysine and a low concentration of PEI modification), and PGPL-H (with lysine and a high concentration of PEI modification). The FTIR and acid orange staining results demonstrated a significant increase in amino content on the scaffolds surface after modification with lysine and PEI (Figure S1, Supporting Information). Subsequently, further cell experiments were conducted to determine the optimal modification concentration of the embolic scaffold (**Figure** 3A). To assess the cell migration ability and biocompatibility of the scaffolds, NIH-3T3 cells were utilized. As demonstrated in Figure 3B, the transwell cell migration assay showed that the PGL group modified with lysine eradicated the toxic effects of crosslinking agents, resulting in significantly better cell migration outcomes compared to the PG group. The increased cell migration observed in the PGPL-L and PGPL-H groups can be credited to the scaffold's several hydrophilic amine groups, which attract cells (Figure 3C). Following a 7-day co-culture, Figure 3D revealed that the PG group displayed significant cytotoxicity, causing a rounded morphology with minimal cell proliferation on the scaffolds. In contrast, the PGL group demonstrated abundant cell proliferation and a spreading morphology on the scaffolds, indicating effective resolution of cytotoxicity due to lysine modification of PG scaffolds. The PGPL-L

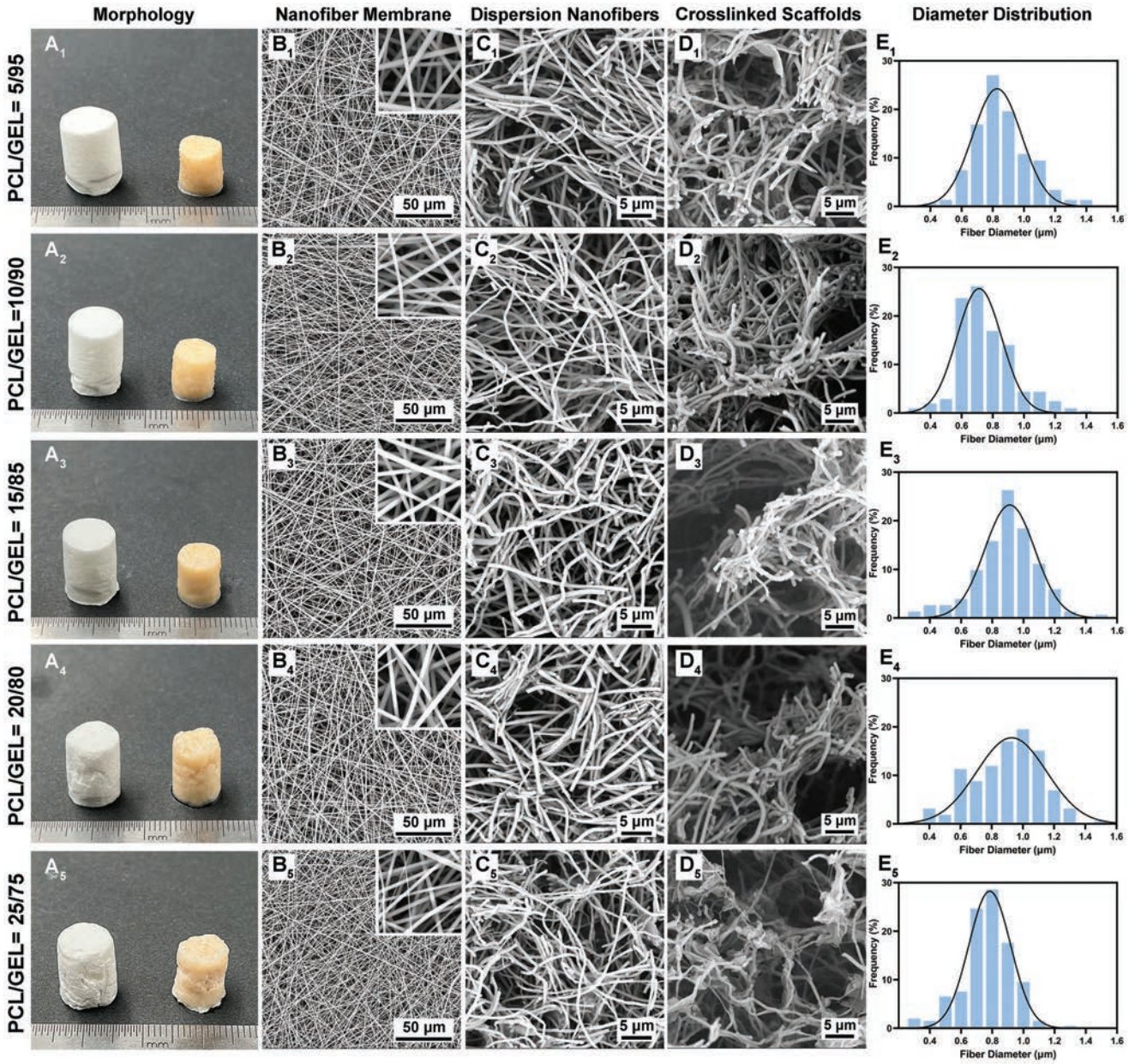

Figure 1. A) Comparison of macroscopic morphology before and after crosslinking of embolic scaffolds. B) SEM images of PCL/GEL nanofiber membrane with different ratios. C) SEM images of dispersion nanofibers after high-speed homogenization (uncrosslinked scaffolds). D) SEM images of crosslinked scaffolds. E) Diameter distribution of PCL/GEL nanofibers with different ratios ($n = 5$).

group demonstrated noteworthy cytocompatibility, presenting a similar rate of cell proliferation and morphology of cell spreading as the PGL group. However, the PGPL-H group displayed a significantly lower cell count than the PGL and PGPL-L groups. Fluorescence results indicated the presence of some dead cells on the seventh day (Figure 3D). The results of the CCK-8 cell proliferation assay and cell SEM also confirmed superior cytocompatibility for the PGL and PGPL-L groups (Figure 3E,F). In order to examine the relationship between embolic scaffolds and vascular endothelial cells, we conducted an assessment of the biological behavior of endothelial cells (HUVEC) on the scaffolds. Our results of CCK-8 cell proliferation as well as live/dead fluorescence staining assays were consistent with those of NIH-3T3 cells (Figure 3G–I; Figure S2A, Supporting Information). In addition, smooth muscle cells (HVSMC) also exhibit good spreading status on PGL and PGPL-L groups (Figure S2B, Supporting Information). Based on these outcomes, we determined the optimal modification conditions for highly elastic modified scaffolds and selected the PGL and PGPL-L groups for the subsequent embolic performance tests.

Next, we conducted physiochemical and chemical characterization of the modified highly elastic embolic scaffolds in the PGL and PGPL-L groups. The water contact angle test results indicated that all groups displayed strong hydrophilicity (Figure S3A,

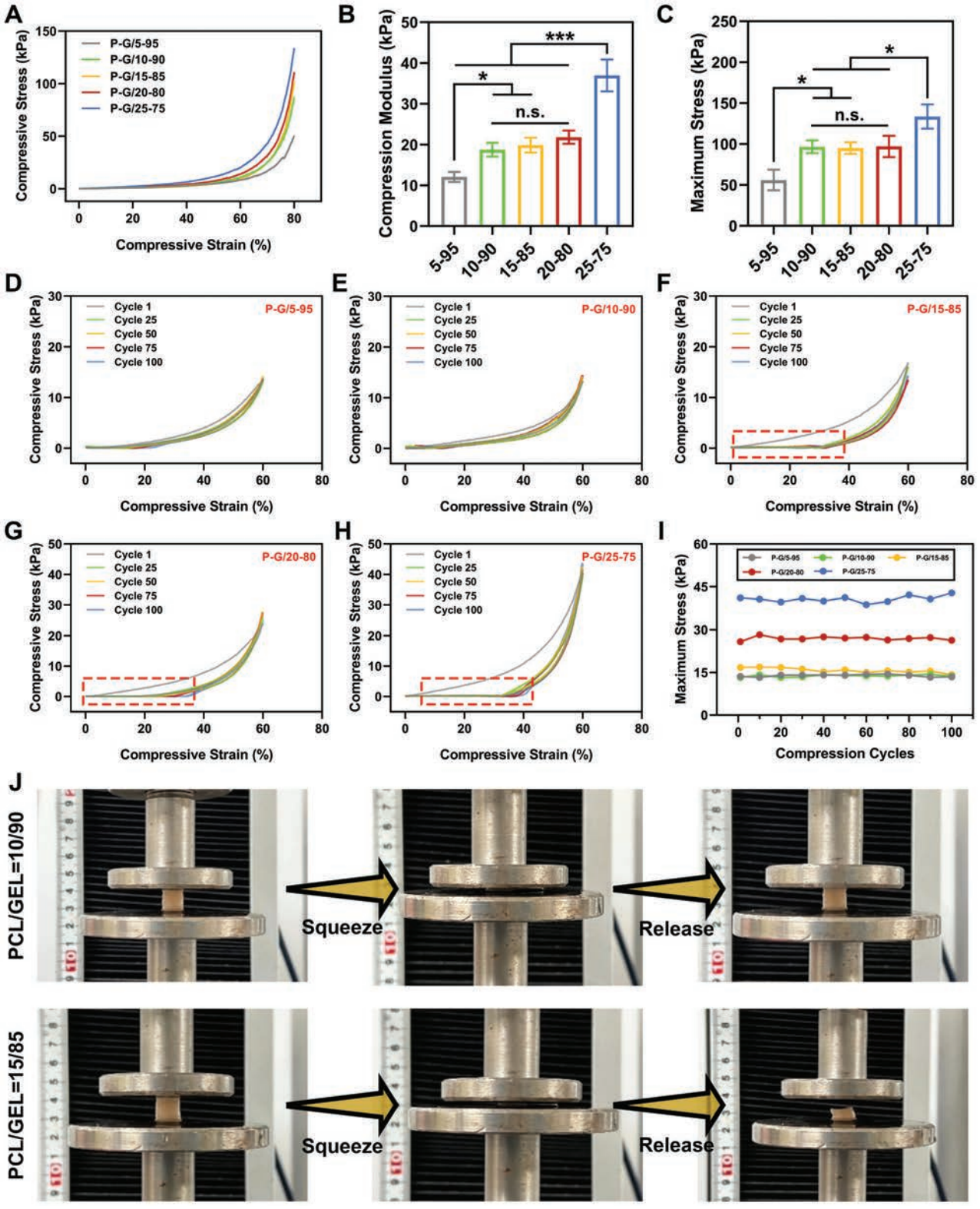

Figure 2. A) Compressive stress–strain curves, B) compressive modulus, C) maximum compressive stress (compressive strain = 80%) of P-G/5-95, P-G/10-90, P-G/15-85, P-G/20-80, P-G/25/75 scaffolds ($n = 3$). D–H) Compressive stress–strain curves of P-G/5-95, P-G/10-90, P-G/15-85, P-G/20-80, P-G/25/75 scaffolds under 100 cycles in the compressive test at 60% strain ($n = 3$). I) The variation of maximum stress with the number of compression test cycles ($n = 3$). J) Macrostructural changes during compression and shape recovery of P-G/10-90 scaffold and P-G/15-85 scaffold. The statistical analysis was performed by using one-way analysis of variance of Tukey's post hoc test, and * means $p < 0.05$, *** means $p < 0.001$.

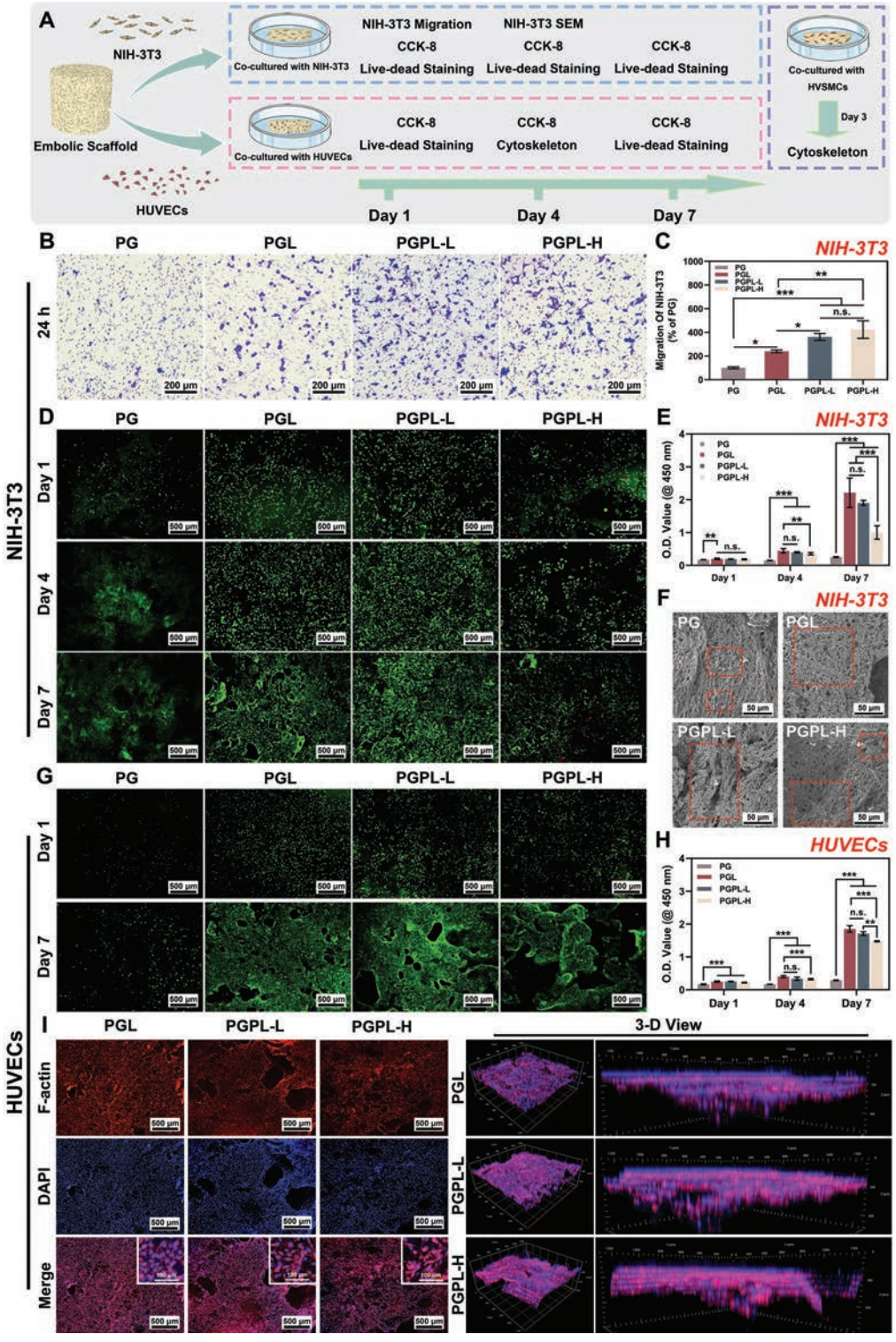

Figure 3. A) Cell compatibility experiment of modified highly elastic embolic scaffolds. B) Migration of NIH-3T3 on PG, PGL, PGPL-L, PGPL-H scaffolds in the transwell assay ($n = 3$). C) Number of migrated NIH-3T3 normalized to PG scaffold. D) Live/dead staining, E) quantitative analysis by CCK-8 assay, and F) SEM images of NIH-3T3 on PG, PGL, PGPL-L, PGPL-H scaffolds for 1, 4, and 7 days ($n = 3$). Live/dead staining (G) and quantitative analysis by CCK-8 assay H) of HUVECs on PG, PGL, PGPL-L, PGPL-H scaffolds ($n = 3$). I) Fluorescent staining of the cytoskeleton of HUVECs after 4 days of culture with PGL, PGPL-L, PGPL-H scaffolds ($n = 3$). The statistical analysis was performed by using one-way analysis of variance of Tukey's post hoc test, and * means $p < 0.05$, ** means $p < 0.01$, *** means $p < 0.001$.

Supporting Information). Both groups had porosity of nearly 60%, with water absorption rates exceeding 500% and achieving saturation within 1 min (Figure S3B–D, Supporting Information). TGA and DTG data indicated that the embolic scaffolds commenced weight loss at 100 °C and exhibited favorable thermal stability (Figure S4A,B, Supporting Information). Results from the degradation study specified that both formulations underwent stable degradation with a mass loss of roughly 10% registered by day 28 (Figure S4C, Supporting Information). Post-degradation mechanical testing was conducted on the PGL and the PGPL-L groups after 14 and 28 days of degradation (Figure S5, Supporting Information). The stress–strain curves are depicted in Figure S5A,G (Supporting Information). The data established that the basic mechanics of both scaffolds after degradation of 14 days were superior compared with the original PG group. The enhancement in mechanics can be attributed to the advanced crosslinking of the scaffolds caused by chemical modification treatments. It was noted that, at day 28, the maximum compressive stress and compressive modulus of both the PGL and PGPL-L groups decreased compared to earlier time points (Figure S5B,C,H,I, Supporting Information). Compression cycling tests were carried out on embolic scaffolds with various degradation time points, and results indicated that the embolic scaffolds had rebound capability after compression with no noticeable permanent deformation (Figure S5D,E,J,K, Supporting Information). No significant stress loss was observed in any of the groups (Figure S5F,L, Supporting Information). Therefore, the embolic scaffold managed to maintain its compression and fatigue resistance mechanical properties even after undergoing a 1 month degradation process. These findings imply that the embolic scaffolds have the prospect of achieving precise in situ embolization in vivo, while maintaining its good mechanical properties even during stable degradation.

The coagulation properties of modified embolic scaffolds were assessed in vitro using 2D nanofibrous membranes with the same composition as PGL (PGL-Membrane group) as a control (**Figure** 4A). Limited platelet and erythrocyte adhesion was seen in the commercial gelatin sponge embolic scaffolds (commercial group), as illustrated in Figure 4B. In comparison to the PGL-Membrane group, the PGL group demonstrated superior platelet and erythrocyte adhesion (Figure 4B). The increased blood contact area in the 3D, highly porous structure of the PGL group contributed to its coagulation effect. The PGPL-L group, on the other hand, showed improved adhesion of platelets and erythrocytes, leading to the formation of a network within the scaffold. The strong, stable positive charge of the PEI component enabled electrostatic adsorption, while the 3D, porous structure of PGPL-L group played a crucial role in this effect. The hemolysis rate test demonstrated no hemolysis in any of the groups (Figure 4C,F). The hemolysis rate in each group was <0.4%, meeting the relevant international standards. This indicates that the scaffolds in all groups exhibited good blood compatibility. The dynamic whole blood coagulation test revealed that the PGPL-L group had the lowest coagulation index (BCI) value (28.95 ± 0.64%), significantly lower than the commercial group (34.78 ± 2.10%), PGL-Membrane group (45.71 ± 2.95%), and PGL group (34.79 ± 0.67%) (Figure 4D,G). Interestingly, in the in vitro blood clotting time determination (BCT), all groups hastened coagulation after interacting with blood and surpassed the control group (370 ± 8.66 s) (Figure 4E,H). The PGL group demonstrated a slightly faster coagulation time (261.33 ± 11.59 s) compared to both the commercial group (290.67 ± 14.29 s) and PGL-Membrane group (272.00 ± 16.37 s). Meanwhile, the PGPL-L group exhibited the shortest BCT (237.33 ± 9.45 s) (Figure 4E,H). This suggests a stronger aggregation effect on platelets and erythrocytes within the highly porous 3D scaffolds with the stabilizing electrostatic adsorption effect of PEI. The PGPL-L group demonstrated rapid blood clot formation, highlighting the potential for effective in vitro coagulation and intravascular embolization.

The embolic scaffold's coagulation mechanism was validated through assessment of its impact on exogenous and endogenous coagulation pathways using prothrombin time (PT) and activated partial thromboplastin time (APTT) evaluations. In comparison to the sample group (Figure 4I,J), which exhibited lower values, the blank group demonstrated higher PT and APTT values of 18.33 ± 1.15 s and 30.67 ± 2.08 s, respectively. The PGL group displayed lower PT values (14.67 ± 1.15 s) compared to both the commercial group (17.33 ± 0.58 s) and the PGL-Membrane group (15.67 ± 0.58 s). Notably, the PT value in the PGPL-L group was significantly lower at 10.67 ± 0.58 s when compared to the other groups (Figure 4I). The APTT test results confirmed these findings, with a significantly lower value of 22.33 ± 0.58 s in the PGPL-L group as opposed to the commercial group (29.33 ± 0.58 s), PGL-Membrane group (26.67 ± 1.53 s), and PGL group (25.67 ± 0.58 s) (Figure 4J). According to the PT and APTT results, the plasma recalcification data showed that the PGPL-L group exhibited the briefest hemagglutination formation time (Figure 4K). These observations suggest that the platelets in the PGPL-L group became more activated and adherent, allowing for intensified aggregation and adsorption effects. Activated platelets rapidly interact with various coagulation factors, accelerating both endogenous and exogenous coagulation and demonstrating a significant procoagulant effect.

Furthermore, embolic scaffolds pose a potential risk of bloodstream infection as interventional devices. In order to evaluate the antimicrobial capacity, we utilized Staphylococcus aureus (Gram-positive bacteria) and Escherichia coli (Gram-negative bacteria) for assessment, as shown in Figure S6 (Supporting Information). Bacterial colonization after 24 h of co-culture with each group is shown in Figure S6A (Supporting Information). The PGPL-L group showed superior antibacterial effects, inhibiting both gram-negative and gram-positive bacteria (Figure S6B,C, Supporting Information). The SEM results demonstrate the bacterial morphology following co-cultivation with scaffolds, indicating a notable disturbance in the PGPL-L group's bacterial membrane structure (Figure S6D, Supporting Information). The main reason for this result is the interaction between the polycation in the PGPL-L group and the negative charge on the bacterial cell membrane. This process resulted in membrane disruption and increased permeability, leading to bacterial death and a more pronounced inhibitory effect.

Next, we tested the ability of the embolic scaffolds to cause vascular embolization in both in vitro and in vivo experiments. As shown in Figure S7 (Supporting Information), a red ink peristaltic pump was utilized to simulate blood flow in vitro. The modified, highly elastic embolic scaffolds exhibited remaining in a fixed position after injection into the simulated blood flow, contrasting with commercial gelatin sponge embolic scaffolds that

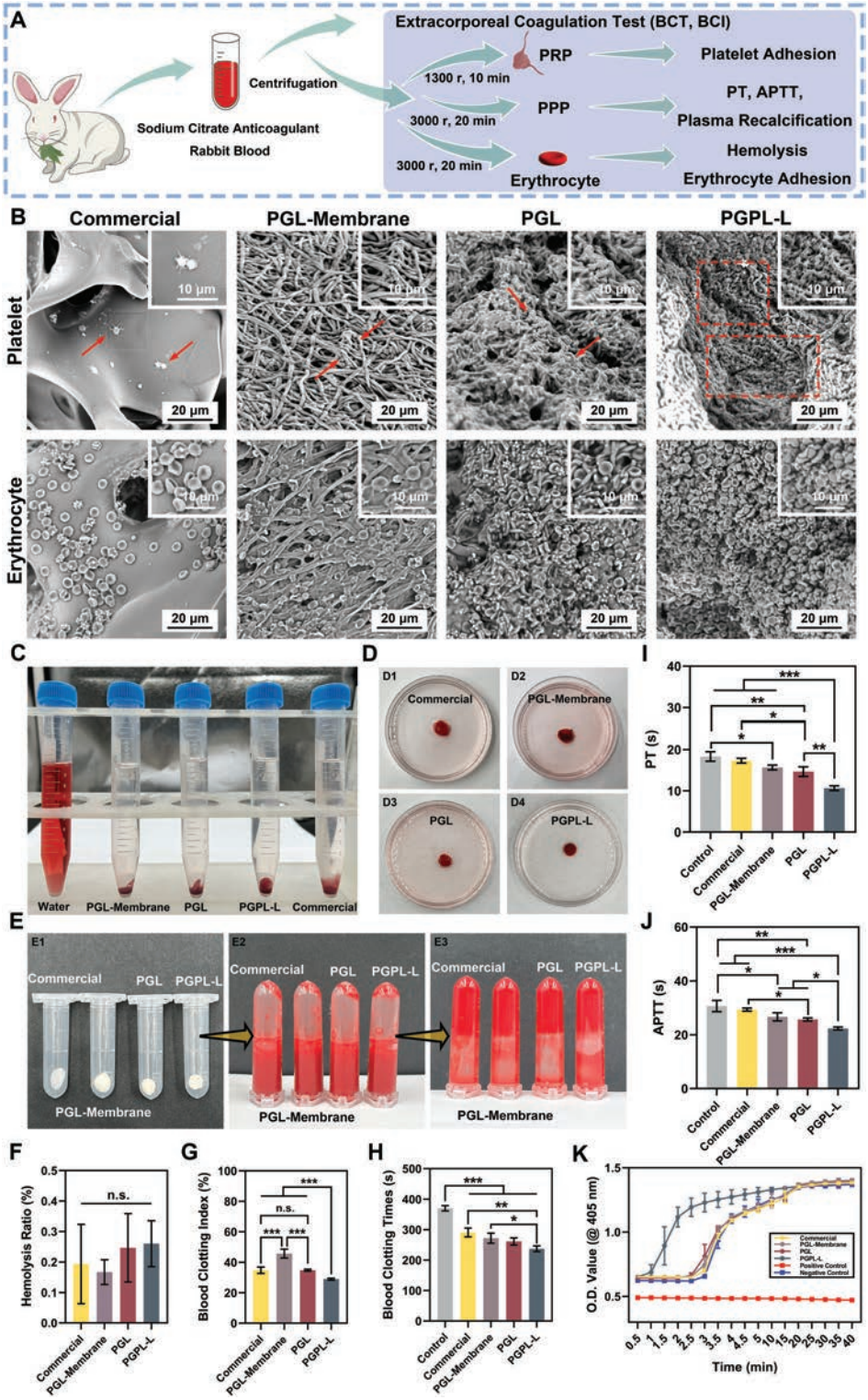

Figure 4. A) In vitro blood coagulation and hemocompatibility properties of embolic scaffolds. B) SEM images of erythrocyte and platelet adhesion on Commercial, PGL-Membrane, PGL, PGPL-L scaffolds ($n = 3$). C) Macrophotograph of hemolysis test, D) dynamic blood coagulation test, and E) blood coagulation time measurement of Commercial, PGL-Membrane, PGL, PGPL-L scaffolds ($n = 3$). F) The hemolysis ratio, G) the blood clotting index (BCI) values, H) the blood clotting times (BCT) values, I) PT, J) APTT values and plasma recalcification profiles (K) of Commercial, PGL-Membrane, PGL, PGPL-L scaffolds ($n = 3$). The statistical analysis was performed by using one-way analysis of variance of Tukey's post hoc test, and * means $p < 0.05$, ** means $p < 0.01$, *** means $p < 0.001$.

tend to collapse when exposed to water. The embolic scaffold, with a diameter of ≈1.5 mm, was extruded smoothly into an injection needle having an internal diameter of ≈0.9 mm (Figure S7A,B, Supporting Information). Upon injection into the simulated blood flow, the scaffold promptly regained its volume and effectively remained in the intended region, causing a significant deceleration of distal blood flow (Figure S7C, Supporting Information). These findings suggest that the embolic scaffold was capable of offering efficient mechanical assistance within the vascular optic lumen of the blood vessel, aligning with the aim of accurate in situ embolization.

In vivo experiments assessed the in situ embolization potential of the embolic scaffold in a rabbit ear embolization model (**Figure 5**A). Histological examinations were conducted in order to conduct this assessment. Analysis of five specific sites at 2- and 4-weeks post-treatment yielded insights into vascular remodeling. Sections 1 and 5 were on autologous vessels near the embolic zone, while Sections 2 and 4 were located at the head and tail of the embolization region. Section 3 referred to the center of the embolism. Sections 1 and 5, located close to the embolic zone on self-originating vessels, demonstrated minimal tissue proliferation at the 2-week time point. While the commercial group displayed some neo tissue in the embolized region, it featured a noticeable cavity (Figure 5B,C,K). A significant expansion in vessel diameter was registered in the embolized zone within the PGL and PGPL-L groups, as illustrated in Figure 5D–G. The results suggest that the embolic scaffold can provide effective mechanical support in the embolized area, filling the entire luminal space completely. Cellular infiltration was observed within the embolic scaffold from Section 2 to Section 5, resulting in significant tissue proliferation and vessel wall thickening (Figure 5L,M). Notably, the PGPL-L group exhibited visible thrombus formation and some tissue proliferation at locus 5 (Figure 5J). Longitudinal cross-section slices of the embolic region showed comparable results to the transverse cross-section (Figure 5H,I). The commercial group demonstrated compressive accumulation within the vessel, resulting in the formation of various microchannels that could likely lead to embolization failure. Conversely, the PGL and PGPL-L groups rendered effective mechanical support within the vessel, causing significant cellular infiltration. Additionally, more thrombus formation was observed in the PGPL-L group, with some areas completing the mechanization process (Figure 5H,I). It was suggested that the enhanced coagulation ability in the PGPL-L group may facilitate accelerated vascular remodeling and successful embolization in the target area.

At 4 weeks, all scaffold groups showed degradation and ongoing proliferation in the lumen. The commercial group experienced fewer material areas, possibly due to displacement or substantial degradation. Both the PGL and PGPL-L groups exhibited degradation from Section 2 to Section 4, along with a further increase in neo tissue (**Figure 6C–F**). The new tissue completely surrounded the embolic scaffold and continued to grow into the material, causing a significant accumulation of tissue within the lumen (Figure 6C–F,K). It was noteworthy that the PGPL-L group demonstrated a superior embolic effect, generating significant tissue neoformation at both Sections 1 and 5, leading to the closure of the lumen (Figure 6E,F). By the 1-month time point, most thrombus components were likely to have completed the process of mechanization, which led to a significantly smaller thrombus area when compared to week 2 (Figure 6I). Longitudinal cross-sections indicated almost complete recanalization of the lumen within the commercial group, except for a minor amount of neo tissue (Figure 6G,H). In contrast, both the PGL group and the PGPL-L group exhibited strong adhesion to the vessel wall, forming stable embolic area. Furthermore, this sustained neo tissue helped maintain the lumen at a nearly 100% embolized area, while also leading to an increase in the thickness of the vessel's intima-media (Figure 6J,L). Endovascular embolization was more significant in the PGPL-L group, where the autologous vessel's lumen near the embolized area nearly closed due to the combined impact of neo tissue and the embolic scaffold (Figure 6G,H).

Endothelial layer reconstruction was assessed in all groups via CD31 immunohistochemical staining (**Figure 7**A,B). The results indicate significant endothelial layer changes during vascular remodeling. The commercial group showed substantial positive CD31 expression after 2 weeks. Endothelial layer reconstruction on the neo tissue surface was observed in the PGL and PGPL-L groups. This reconstruction took place in specific areas where the embolic scaffolds remained in close contact with the vessels, reducing the chance of microvascular channel formation (Figure 7A,I). After 4 weeks, with revascularization in progress, the distribution of the endothelial layer in the commercial group was similar to that of natural vasculature, except for a few areas with neovascularization (Figure 7B,J). In both the PGL and PGPL-L groups, the endothelial layer underwent reconstruction on the neovascularized tissue surface. The neo tissue was extensively deposited and new blood flow pathways were not formed by the endothelium.

Macrophage infiltration was assessed in all groups through CD68 immunohistochemical staining. After 2 weeks, strong CD68-positive expression was detected at locus 3 in the commercial, PGL, and PGPL-L groups. A significant macrophage infiltration in the lumen was also observed (Figure 7C–E,K). These findings indicate that macrophages may participate in material degradation and stimulate new tissue formation in the embolic region. Simultaneously, the degradation process impacted the vessel wall, resulting in significant CD68-positive expression (Figure 7C–E,L). Notably, CD68-positive expression at locus 2 was marginally less than that observed at locus 3, potentially due to faster material degradation at the embolized area's borders and increased tissue neogenesis completion (Figure 7C–E). At the 4-week mark, all groups exhibited significantly lower CD68 expression in the vessel wall and lumen due to the deposition of neo tissue and material degradation (Figure 7F–H). Meanwhile, at Section 3, material persisted, necessitating macrophages for continuous tissue regeneration and material breakdown (Figure 7F–H,M). The PGPL-L group successfully embolized the lumen at Section 2. The neo tissue wholly blocked the lumen, and the vessels and lumen showed minimal CD68 expression (Figure 7H,M,N). A decrease in inflammatory expression was recorded in the embolized region. After implanting the embolic stent into the vessel during embolization, macrophages infiltrated the area heavily, and the material started to degrade. Simultaneously, new tissue deposition commenced, and CD68 expression decreased gradually with the embolization process. In conclusion, the findings indicate that

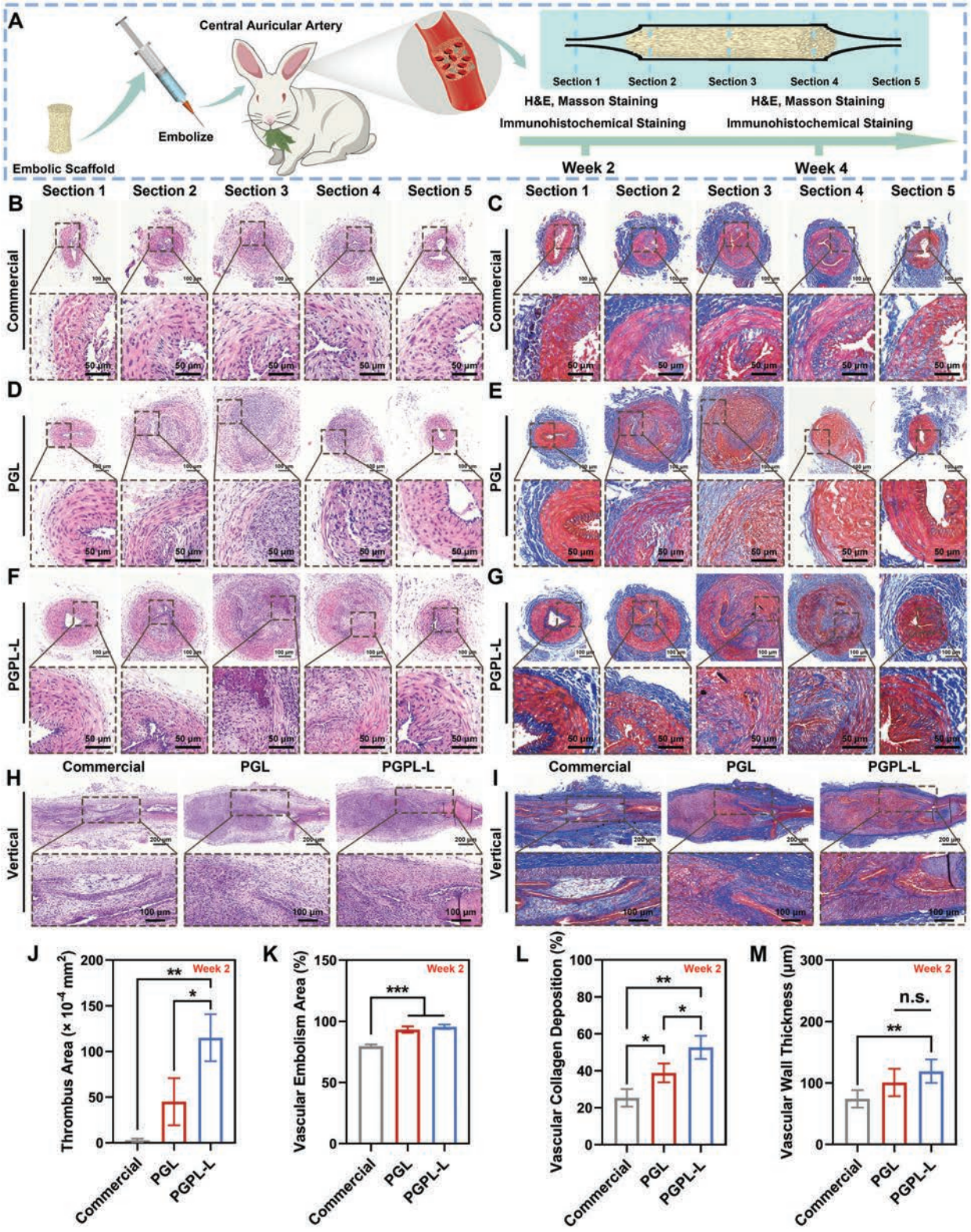

Figure 5. A) Modified embolic scaffold for embolization in rabbit ears. B,D,F) H&E staining and C,E,G) Masson trichrome staining of five sections of B,C) Commercial scaffolds, D,E) PGL scaffolds, and F,G) PGPL-L scaffolds at week 2 ($n = 5$). H,I) H&E staining and Masson trichrome staining of Commercial, PGL, PGPL-L scaffolds at week 2 (Vertical) ($n = 5$). J) Thrombus area, K) vascular embolism area, L) collagen deposition, and M) vascular wall thickness quantification of Commercial, PGL, PGPL-L scaffolds ($n = 5$). The statistical analysis was performed by using one-way analysis of variance of Tukey's post hoc test, and * means $p < 0.05$, ** means $p < 0.01$, *** means $p < 0.001$.

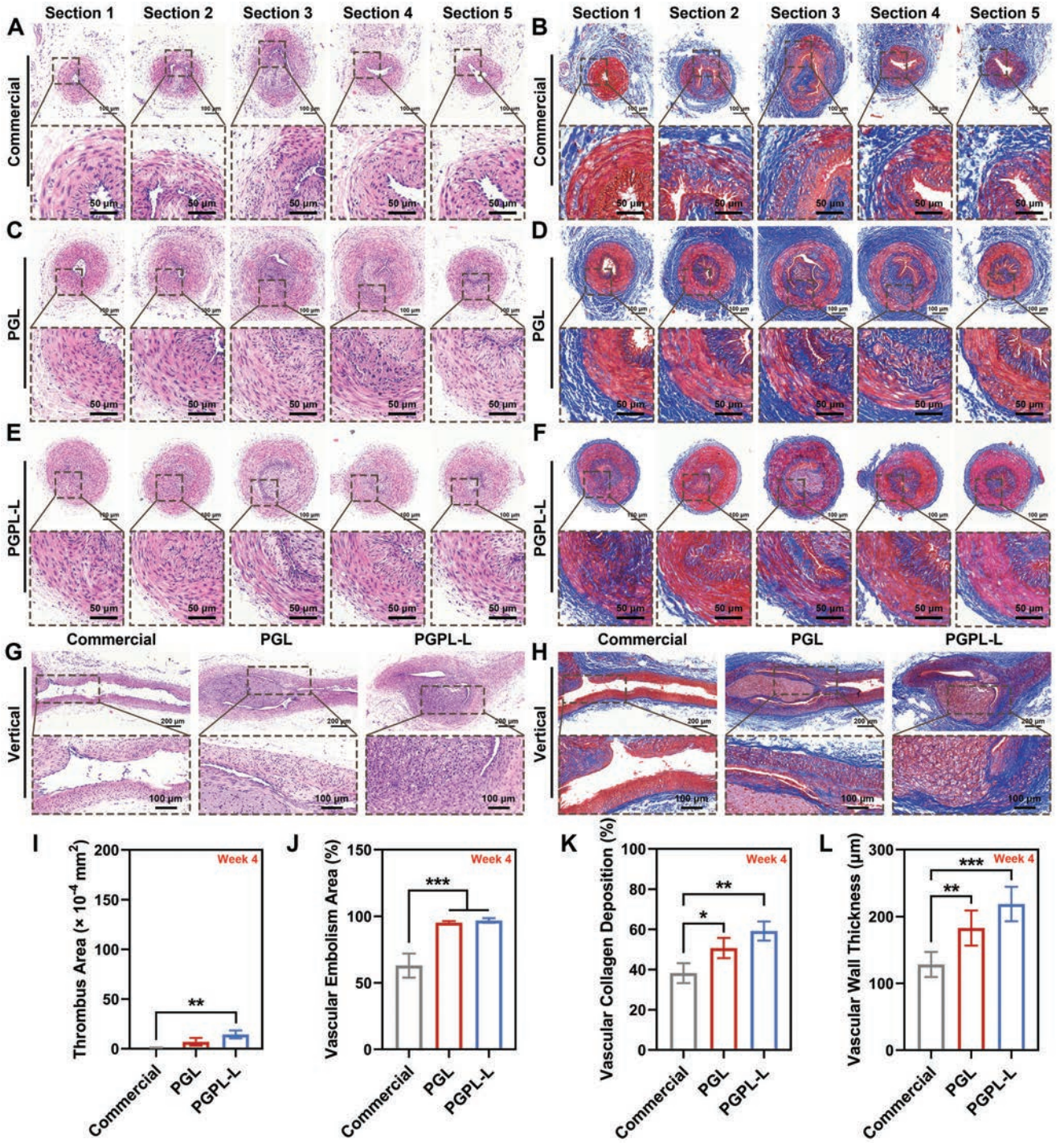

Figure 6. A,C,E) H&E staining and B,D,F) Masson trichrome staining of five sections of A,B) Commercial scaffolds, C,D) PGL scaffolds, and E,F) PGPL-L scaffolds at week 4 ($n = 5$). G,H) H&E staining and Masson trichrome staining of Commercial, PGL, PGPL-L scaffolds at week 4 (Vertical) ($n = 5$). I) Thrombus area, J) vascular embolism area, K) collagen deposition, and L) vascular wall thickness quantification of Commercial, PGL, PGPL-L scaffolds ($n = 5$). The statistical analysis was performed by using one-way analysis of variance of Tukey's post hoc test, and * means $p < 0.05$, ** means $p < 0.01$, *** means $p < 0.001$.

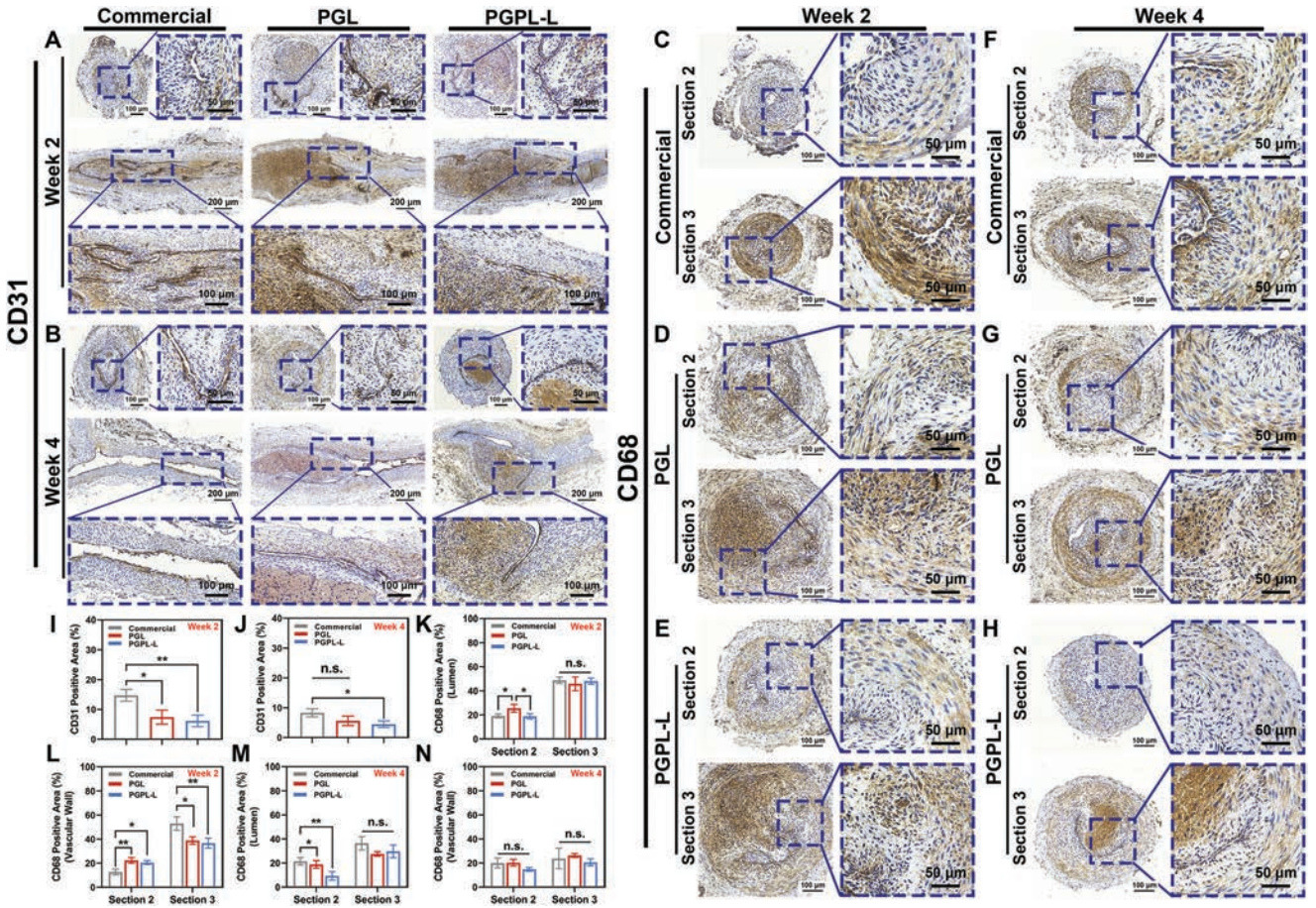

Figure 7. A,B) Immunohistochemical staining of Commercial, PGL, PGPL-L scaffolds (CD31) ($n = 5$). C–H) Immunohistochemical staining of Commercial, PGL, PGPL-L scaffolds on Section 2 and Section 3 (CD68) ($n = 5$). I,J) CD31 positive area of Commercial, PGL, PGPL-L scaffolds ($n = 5$). CD68 positive area of Commercial, PGL, PGPL-L scaffolds at K,L) week 2 and M,N) week 4 in (K,M) lumen and L,N) vascular wall ($n = 5$). The statistical analysis was performed by using one-way analysis of variance of Tukey's post hoc test, and * means $p < 0.05$, ** means $p < 0.01$.

the modified highly elastic embolic scaffold facilitates stable embolization throughout the embolization period.

3. Discussions

The study aimed to achieve precise and efficient vascular embolization using a modified highly elastic embolic scaffold. The scaffold can be compressed to a size small enough to enter the vessel through an interventional procedure and quickly regain its volume after reaching the target area for precise in situ embolization. To prevent off-target material flow or fragmentation after intervention in the vasculature, appropriate crosslinking methods were used for in vitro construction and molding. Five ratios of PCL/GEL nanofibers were used to prepare 3D scaffolds. The scaffolds were cast and lyophilized after high-speed homogenization. Then, the scaffolds were crosslinked with glutaraldehyde solution to improve their mechanical properties. The mechanical property test results showed that the scaffolds were structurally intact and had excellent compression resistance under compression up to 80% strain. Embolic scaffolds are subjected to mechanical compression during delivery through the microcatheter to the target embolic region. Additionally, the implanted embolic scaffolds are continuously exposed to physiologic pressure from the vasculature. These make it critical for embolic scaffolds to have stable anti-fatigue properties. In this study, the fatigue resistance of the highly elastic embolic scaffold was tested through cyclic compression. The study found that there was variability among the groups, and the PG group (P-G/10-90) exhibited more desirable fatigue resistance properties. As a result, this group was chosen for further investigation.

Biocompatibility is a crucial indicator for implants and embolic scaffolds. Glutaraldehyde is a commonly used natural crosslinking agent, but its cytotoxicity tends to be high.[28] Therefore, highly elastic embolic scaffolds cross-linked by glutaraldehyde are less biocompatible, despite having better mechanical properties. In this study, the amino group of lysine was used to combine with the residual glutaraldehyde-free aldehyde group to address its biotoxicity. To further enhance the functionality of the embolic scaffolds, the scaffolds were modified with PEI in this study. PEI possesses a strong positive surface charge, and its polycationic properties effectively enhance the procoagulant and antimicrobial capabilities of the scaffold. In addition, its abundant amino groups can be functionalized by chemical modification. This makes the embolic scaffolds have more potential for imaging and

drug loading. However, excessive polycation may be potentially biotoxic. Therefore, we confirmed the modified concentration of PEI in this study through in vitro cellular experiments. The results indicate that the modified treatments effectively addressed the toxicity of glutaraldehyde residue. Meanwhile, it is recommended to use low concentrations of PEI-modified scaffolds for better biocompatibility. The cytofluorescence staining results indicate that cells exhibit improved 3D infiltration and proliferation behavior on the modified embolic scaffolds. This perfectly compounds the clinical need, as usually embolic target areas are accompanied by degradation of the material after embolization, and neo tissue deposition through massive cellular infiltration needs to be achieved in time to maintain embolization.[29] Physicochemical characterization tests showed good hydrophilicity and porosity of the PGL group and PGPL-L. The modified embolic scaffolds maintained good compressive and fatigue strength mechanical properties in in vitro degradation tests for up to 28 days. The hemolysis rate experiment results indicated that all groups of modified embolic scaffolds had a hemolysis rate of <0.4%, demonstrating good hemocompatibility.[30] The PGPL-L group exhibited the most significant erythrocyte and platelet adhesion effect and could enhance the procoagulant effect by accelerating both endogenous and exogenous coagulation. In conclusion, the in vitro results suggest that modified embolic scaffolds may be able to physically obstruct blood flow in vessel lumens to achieve precise embolization due to their excellent mechanical properties. Additionally, the good biocompatibility may induce significant cellular infiltration and promote neo tissue deposition. During this process, the altered scaffold may also cause thrombus formation in the embolic region. Furthermore, the PGPL-L group exhibited superior antimicrobial efficacy, reducing the risk of bloodstream infections when the material enters the vessel. Therefore, the PGPL-L group demonstrated greater potential for use as an embolic agent in in vitro experiments.

In vivo experiments, PGPL-L group produced a substantial amount of neo tissue, leading to complete occlusion of the vessel lumen. Furthermore, the neo dense collagen tissue fully enveloped the modified embolization scaffold. This procedure enhances the safety of the embolization process and reduces the risk of fragment displacement during material degradation. The modified embolic scaffold demonstrated better embolization due to its good mechanical support in the lumen. In contrast, the commercial group showed proliferation of endothelial cells and formation of microvascular channels, which led to revascularization failure and embolization failure at week 4. CD68 immunohistochemistry was used to evaluate cellular infiltration and tissue regeneration at Sections 2 and 3. During the early phase of embolization, all groups showed a large amount of CD68-positive expression. A significant macrophage infiltration was observed in the central region of embolization, which is consistent with the typical characteristics of biomaterials after implantation.[31] This infiltration promotes material degradation and creates space for neo tissue deposition. At Section 2, we observed more neo tissue deposition with less residual scaffold material due to faster macrophage infiltration. The modified embolic scaffold maintained almost complete occlusion without luminal recanalization due to degradation. At week 4, degradation and tissue neovascularization continued. Compared to week 2, CD68-positive expression significantly decreased in all groups. Undegraded material remained in the central embolic region of the modified embolic scaffold, resulting in some macrophage infiltration at Section 3. In the PGPL-L group, the region at Section 2 was almost completely occluded, and CD68 positivity was nearly absent in both the vessel wall and lumen at this section. This indicates that the process of embolization was safe and stable. Complete occlusion of the embolized area was achieved due to complete material degradation, and the inflammatory state also subsided. Therefore, with effective mechanical support of the scaffold during the pre-embolization phase, maintenance of the balance between material degradation and neo tissue regeneration in the mid-term phase, and the formation of stable proliferative tissue in the late phase of scaffold degradation, the PGPL-L can provide an ideal embolism process to exert its embolic effect.

In summary, the modified highly elastic embolic scaffolds exhibit excellent mechanical properties that facilitate interventional delivery to the target area for precise embolization. The scaffolds also maintain a good balance between the embolization process, material degradation, and neo tissue replacement after embolization. Additionally, the PEI-modified scaffolds demonstrated superior procoagulant ability and embolic effect in vivo. However, future studies will address the current design's shortcomings. For instance, the modified embolic scaffold lacks visualization, making it challenging to detect its embolic status in vivo. This issue can be resolved by adding a contrast agent. The modified embolic scaffolds contain numerous branched amino acid groups that enable chemical grafting of contrast agents, including pantothenic acid, thereby providing visualization capabilities. Further in vivo validation is required to address key issues, such as the degradability of modified embolic scaffolds and the duration of occluded regions. Future studies should evaluate the long-term embolic effect of modified embolic scaffolds in vivo.

4. Conclusion

This study presents the construction of a highly elastic embolic scaffold using PCL/GEL nanofibers that meet the requirements for precise in situ embolization due to their good mechanical properties and fatigue resistance. The biocompatibility of the Lys- and PEI-modified embolic scaffolds was excellent, and the functionality of the modified embolic scaffolds, such as procoagulant properties, was further improved. Additionally, the modified embolic scaffold retained its anti-fatigue properties after a 28-day degradation test, ensuring its ability to embolize in vivo without the risk of dislocation. Histological staining demonstrated the scaffold's effective embolic properties in vivo, with stable deposition of neo tissue during material degradation maintaining ≈100% of the vessel lumen. In the PGPL-L group, the embolic region achieved complete occlusion and the inflammatory state nearly disappeared, demonstrating a more desirable embolic process. The modified highly elastic embolic scaffolds were designed and show great potential for clinical embolization applications.

5. Experimental Section

Materials: L-Lysine (Purity ≈98%) was purchased from Aladdin (China). Gelatin (Type A), polyethyleneimine (PEI, M_w ≈25 000, branched),

polycaprolactone (PCL, M_w ≈80 000) was purchased from Sigma–Aldrich (USA).

Preparation of PCL/GEL Nanofiber Membrane and Embolic Scaffolds: Preparation of PCL/GEL nanofiber membrane: 0.9, 0.96, 1.02, 1.08, and 1.14 g of gelatin (GEL) were dissolved in 10 mL of hexafluoroisopropanol (Aladdin) and stirred at high speed until the gelatin was completely dissolved. Then 0.3, 0.24, 0.18, 0.12, and 0.06 g of PCL were added to the above gelatin solutions and stirred at high speed until the PCL was completely dissolved. Finally, 15 µL of acetic acid (Aladdin) was added to each solution and stirred at high speed until the solution was thoroughly clarified to obtain the electrospinning solution (PCL to GEL ratios were: 25–75, 20–80, 15–85, 10–90, 5–95). Then, the electrospinning solution was used to prepare the PCL/GEL nanofiber membrane according to the following parameters: Needle size was 20-G. Voltage was 14 kV. Push rate was 1.5 mL h^{-1}, and the distance between needle and collector was 15 cm. Finally, the obtained PCL/GEL nanofiber membrane was vacuum dried for 12 h.

Preparation of Embolic Scaffolds: Four grams of PCL/GEL nanofiber membrane was cut into 1 × 1 cm pieces and placed in 100 ml of tert butanol (Aladdin). Subsequently, it was homogenized using a high-speed homogenizer at 10 000 rpm to obtain dispersion nanofibers. The dispersion nanofibers were then transferred to molds and freeze-dried for 48 h to obtain uncrosslinked scaffolds. The uncrosslinked scaffolds were crosslinked by immersion in 5% glutaraldehyde (Aladdin) solution for 15 min, followed by washing three times with deionized water. Finally, the crosslinked scaffolds were obtained.

Morphology Characterization: The macro and microscopic morphology of PCL/GEL nanofiber membrane, uncrosslinked scaffolds, and crosslinked scaffolds with different ratios (PCL to GEL ratios were: 25–75, 20–80, 15–85, 10–90, 5–95), which were photographed with a digital camera and scanning electron microscopy (SEM, Phenom, Netherlands) at an accelerating voltage of 5 kV, respectively.[32] The corresponding diameter distribution of PCL/GEL nanofiber membrane samples were measured by Image J software.

Mechanical Properties: Mechanical properties of the crosslinked scaffolds (P-G/25-75, P-G/20-80, P-G/15-85, P-G/10-90, P-G/5-95) with different ratios were tested in the wet state with a universal material testing machine with a 200 N load cell (Instron 5567, Norwood, MA). The samples were subjected to unconfined uniaxial compression at a constant crosshead speed of 2 mm min^{-1} up to 80% strain, the compression strength and compression modulus were calculated from the compression curves ($n = 3$). The samples were tested with 100 compression tests at a rate of 2 mm min^{-1} and a maximum load strain of 60%, and the compressive strength was calculated after every ten cycles to determine the mechanical loss during cyclic compression.[33] After evaluating the mechanical properties, the optimal ratio was selected and termed as highly elastic embolic scaffolds for pending modification treatment (PG).

Modification of Embolic Scaffolds: PEI-modified solutions were prepared by dissolving PEI in isopropanol/water (1:1, v/v) at low (1.25 mg mL^{-1}) and high (2.5 mg mL^{-1}) concentrations. The highly elastic embolic scaffolds (PG) were aminated by immersing in PEI-modified solution for 15 min with stirring, followed by immersing in 5% Lys solution (pH 3–4) with stirring for 6 h to eliminate the toxic effects of free aldehyde groups using the Schiff base reaction. Finally, the embolic scaffolds were immersed in 0.5% $NaBH_3CN$ (AR, Aladdin) solution with stirring for 15 min to stabilize the branched amino groups that attached to the scaffolds by reductive amination reaction. The modified embolic scaffolds were obtained (modified at low concentration as PGPL-L and at high concentration as PGPL-H). In order to study the effect of amination on embolic scaffolds, PGL embolic scaffolds were treated with Lys and $NaBH_3CN$ solution, but without PEI-modified solutions.

FTIR, TGA, and DTG: Fourier transform infrared spectra (FTIR, Nicolet-760, Madison) was used to characterize the compositional analysis of the embolic scaffolds (PG, PGL, PGPL-L, and PGPL-H) in the 500–4000 cm^{-1} range, while uncrosslinked scaffold was characterized as control group.

Thermogravimetric analysis (TGA) of embolic scaffolds (PG, PGL, PGPL-L, and PGPL-H) was performed using a thermogravimetric analyzer (PerkinElmer Corporate Management Co., Ltd., TGA8000, Shanghai, China) under nitrogen at temperatures ranging from room temperature to 800 °C with a heating rate of 5 °C min^{-1}. Thermogravimetric parameters were analyzed with TGA curves.[34]

Porosity, Water Absorption, and Water Contact Angle: The porosity of the embolic scaffolds was determined by the liquid displacement method referring to the previous method.[35] The diameter (d), height (h), and weight (m_1) of the dry scaffolds were first measured, and then the scaffolds were immersed in 200-proof ethanol. After removal from ethanol, the scaffolds were reweighed (m_2). The porosity was calculated by the following formula:

$$porosity\ (\%) = \frac{100 \times (m_2 - m_1)}{\rho_{ethanol} \times (d/2)^2 \times h \times \pi} \quad (1)$$

The mass of the dried scaffold was measured (m_a) and incubated in deionized water. At different time points, the scaffolds were extracted and weighed (m_b). The water absorption capacity was calculated as follows:[36]

$$Water\ absorption\ capacity\ (\%) = \frac{m_b - m_a}{m_a} \times 100\% \quad (2)$$

Five replicates were measured for each scaffold.

The water contact angle of the embolic scaffolds was measured by a contact angle analyzer (DSA30, KRUSS, Germany)[37] ($n = 3$).

Amino Quantification: Acid Orange II staining was used to quantify the amine content of the embolic scaffolds and the corresponding standard curves were plotted and characterized according to the following scheme. Briefly, 10 mg of each group was first immersed in 2 mL of Acid Orange II deionized water solution (pH 3, concentration 500 µmol L^{-1}, 0.0875 g of Acid Orange II dissolved in 500 mL of deionized water) and reacted for 12 h. The samples were then removed and washed three times with acidic aqueous solution (pH 3). The water on the surface of the sample was drained and immersed in 1 mL of aqueous NaOH solution (pH 12) to release the Acid Orange II adsorbed on the surface of the sample by electric charge. After 30 min, the absorbance value of released solution was measured with an enzyme counter at 485 nm, and the amount of adsorption on the surface of the samples was calculated from the standard curve of the formulated Acid Orange II.

Degradation and Degradation Mechanical Properties: The in vitro degradation properties of the embolic scaffolds were determined. The samples were weighed (m_0) and incubated in PBS at 100 rpm, 37 °C. Samples were harvested at different time points, lyophilized, and weighed (m_t). The degradation rate was calculated as follows:

$$Degradation\ Rate\ (\%) = \frac{m_0 - m_t}{m_0} \times 100\% \quad (3)$$

The cyclic compression performance of the degraded scaffolds was determined at different time points ($n = 3$).[32,38]

Antibacterial Test: The antibacterial activity of embolic scaffolds was evaluated against two commonly used bacteria: Gram-negative *Escherichia coli* (*E. coli*), and Gram-positive *Staphylococcus aureus* (*S. aureus*). The bacteria were cultured in Mueller–Hinton broth (MHB) at 37 °C. After the scaffolds were sterilized by UV light for 24 h, 100 µL of bacteria (10^5 CFU mL^{-1}) were introduced onto each scaffold and incubated for 24 h at 37 °C. The scaffolds were transferred to PBS, diluted after agitation, and plated on Luria–Bertani agar plates. Colonies were photographed and counted after incubation for 24 h at 37 °C. PBS-seeded bacteria were used as controls.

Blood Compatibility of Embolic Scaffolds: In this part of the experiment, the group of 2D nanofiber membranes with the same composition as PGL was introduced (PGL-Membrane). PGL-Membrane was introduced to evaluate the additional advantage of the structure of the modified embolic scaffolds on coagulation. The in vitro hemostatic capacity was evaluated using the dynamic whole blood coagulation test, and the coagulation index (BCI) was determined for each group was determined.[39] Discs weighing ≈10 mg were prepared from the materials of each group, placed in Petri

dishes, and preheated at 37 °C for 10 min. Then, 50 µL of sodium citrate anticoagulated rabbit blood was dropped on the surface of the samples, followed immediately by 10 µL of $CaCl_2$ solution (0.2 M). The Petri dishes were then incubated on a shaker at 37 °C to facilitate interaction between the blood and the material. After 5 min, 5 mL of deionized water was gently added to wash away the unclotted blood. A final 5-min incubation on a 37 °C shaker was performed to collect free erythrocytes. The absorbance of 50 µL of sodium citrate anticoagulated rabbit blood in 5 mL of deionized water was used as a negative control value. The absorbance of the hemoglobin solution was recorded using an enzyme marker at 540 nm ($n = 3$). The BCI was calculated as follows:

$$BCI\ (\%) = \frac{I_S}{I_C} \times 100\% \quad (4)$$

where I_S represents the absorbance of the sample and I_C represents the absorbance of the negative control.

The whole blood clotting time of the material was tested as follows (BCT).[40] Briefly, 1 mL of sodium citrate anticoagulated rabbit blood was added to a centrifuge tube containing the material, followed by 30 µL of $CaCl_2$ solution (0.25 M). The tube was inverted every 15 s and blood clotting was recorded each time ($n = 3$) (Control: no materials added).

Hemolysis test was performed using a 2% (v/v) suspension of erythrocyte.[19] Fresh whole blood (containing sodium citrate) from New Zealand rabbits was centrifuged at 3000 rpm for 20 min. The resulting erythrocyte suspension was washed three times with saline and diluted to a 2% (v/v) suspension. Each scaffold was incubated in 10 mL of saline at 37 °C for 30 min, and 0.2 mL of erythrocyte suspension was dropped in and gently mixed. After incubation for 1 h at 37 °C, the scaffolds were centrifuged at 3000 rpm for 10 min, and the absorbance of the supernatant was measured at 540 nm with a microplate reader (Multiskan MK3, Thermo Fisher Scientific). 0.9% normal saline and deionized water were used as negative and positive controls, respectively.

Platelet adhesion: Platelet-rich plasma (PRP) was prepared by centrifugation of anticoagulated whole blood at 1300 rpm for 10 min and separation of the upper plasma layer. Samples were incubated with 200 µL PRP for 30 min at 37 °C. Erythrocyte adhesion: Anticoagulated whole blood was centrifuged at 3000 rpm for 20 min, erythrocytes were extracted, diluted in saline and incubated with samples for 5 min at 37°C. The finished incubated samples were washed sufficiently with PBS to remove unadhered platelets and erythrocytes, then fixed with 4% paraformaldehyde and dehydrated with gradient ethanol. The morphology of platelets and erythrocytes attached on the samples was observed by SEM.[41]

The anticoagulant capacity of the scaffolds was assessed by prothrombin time (PT) and activated partial thromboplastin time (APTT).[42] Anticoagulated whole blood was centrifuged at 3000 rpm for 20 min, and the supernatant was taken to obtain platelet-poor plasma (PPP). The scaffolds were placed in 100 µL of PPP and incubated at 37 °C for 2 min. Then 100 µL PT reagent was added to the incubated sample, and the PPP clotting time was recorded as PT ($n = 3$). 100 µL of APTT reagent was added to the incubated sample, and the sample was incubated for 3 min at 37 °C. 100 µL of 0.025 M $CaCl_2$ solution was added, and the PPP clotting time was recorded as APTT ($n = 3$). Plasma recalcification experiments were performed as in previous studies.[43] The material was placed in a 24-well plate, and 500 µL of PPP was added to each well and incubated for 1 h. Then, 100 µL of PPP was transferred from each well to be added to the 96-well plate, and 100 µL of $CaCl_2$ solution (0.025 M) was quickly added. The PPP-incubated blank plate was added with $CaCl_2$ solution as a negative control, and the $CaCl_2$ solution without $CaCl_2$ solution was used as a positive control. Finally, the absorbance of the 96-well plate was measured at 405 nm every 30 s for 45 min (Control: no materials added).

Cytocompatibility of Embolic Scaffolds: The cytocompatibility of the embolic scaffolds was evaluated in vitro. NIH-3T3 fibroblasts, Human vascular smooth muscle cells (HVSMCs) and human umbilical vein endothelial cells (HUVECs) were supplied by the Cell Bank of the Chinese Academy of Sciences. Cells were maintained and expanded in DMEM medium supplemented with 10% fetal bovine serum (FBS) and 1% penicillin/streptomycin at 37 °C and 5% CO_2 in an incubator. The medium was changed every other day.

Embolic scaffolds (10 mm diameter, 1 mm thickness) were sterilized by ultraviolet irradiation for 24 h and then seeded with cells on the surface at a density of 2×10^4 cells cm^{-2}. Cells were cultured in complete medium and were changed every other day.

At days 1, 4, and 7, cell growth on embolic scaffolds was detected using the Cell Counting Kit-8 (CCK-8) according to the manufacturer's protocol. Cells on scaffolds were stained with calcein-AM and propidium iodide to visualize live and dead cells respectively, and imaged with a fluorescence microscope (DMi 8, Leica, Germany). Cell-seeded scaffolds were fixed with 4% paraformaldehyde and dehydrated with gradient alcohol and were imaged with SEM to visualize cell adhesion.

The ability of the scaffolds to support cell migration was evaluated using a transwell assay. In brief, the scaffold was placed in the lower transwell chamber (Sigma–Aldrich), and cells (1×10^4 cells cm^{-2}) were seeded on the upper chamber. After incubation for 24 h, cells passing through the transwell membrane were stained with 0.1% (w/v) crystal violet (Sigma–Aldrich). The migrated cells were washed with PBS and observed by a light microscopy. Cell migration was quantified using Image J ($n = 3$).

The morphology of HVSMCs and HUVECs on the embolic scaffolds was observed by confocal laser microscopy. The scaffolds were collected and fixed with 4% paraformaldehyde, permeabilized with 0.1% Triton X-100. After rinsing with PBS, these scaffolds were incubated with rhodamine-conjugated phalloidin for 20 min and with 40, 6 dimethyl diamidino-2-phenylindole (DAPI) for 5 min. The samples were then imaged under a laser confocal microscope (LSM 700, Carl Zeiss) to show the 3D distribution and the morphology of HVSMCs and HUVECs on the scaffolds.

In Vivo Assessments of Embolic Scaffolds: New Zealand rabbits (2-3 kg, male) were used to evaluate in vivo embolic capacity assessment.[44] The rabbit ears were first shaved, and the ears were sterilized with 75% ethanol. Local anesthesia was then applied to the dorsum of the ear avoiding blood vessels. An incision was made in the skin of the ear to identify the central ear artery. Commercial (Alicn, China, 1.4–2 mm), PGL (diameter: 1.5 mm, length: 2 mm), and PGPL-L (diameter: 1.5 mm, length: 2 mm) were mixed with an aqueous solution of glycerol (glycerol: water = 1:1) and squeezed into the injection needle and then slowly infused. Finally, the wound was sutured after pressing the injection site until bleeding stopped. The status of rabbit ear embolism was observed and photographed at weeks 0, 2, and 4. All materials and instruments used during the animal experiments were sterilized.

The central ear artery tissues were harvested at the 2 and 4 weeks and fixed in 4% paraformaldehyde. Then, five typical sections were selected for histological sectioning from the starting area to the ending area of the embolic site. Evaluate indicators such as thrombosis formation, deposition of new tissue and degree of vascular occlusion in the embolic area by H&E and Masson staining. Finally, further evaluation of angiogenesis and macrophage infiltration in the embolic regions of each group was performed using CD31 and CD68 immunohistochemistry staining. All the animal experiments were reviewed and approved by the Animal Experimental Ethical Inspection Form Shanghai Songjiang Chedun Experimental Animal Breeding Farm Co., Ltd. (No: 2023092001).

Statistical Analysis: Data were presented as mean ± standard deviation and were analyzed by using one-way analysis of variance of Tukey's post hoc test. Comparison of the two groups was performed by t-test. Statistical significance was considered at $p < 0.05$, and * means $p < 0.05$, ** means $p < 0.01$, *** means $p < 0.001$ (GraphPad Prism 8.0 software, USA).

Supporting Information

Supporting Information is available from the Wiley Online Library or from the author.

Acknowledgements

P.C., L.C., and Y.D. contributed equally to this work. This work was supported by the Fundamental Research Funds for the Central Universities

(No. 2232023D-10), the National Natural Science Foundation of China (No. 82202685), the Science and Technology Commission of Shanghai Municipality, China (No. 20DZ2254900), the Sino German Science Foundation Research Exchange Center, China (No. M-0263), and the China Education Association for International Exchange (No. 2022181). This project was also supported by the Researchers Supporting Project , King Saud University, Riyadh, Saudi Arabia (No. RSP2024R65).

Conflict of Interest

The authors declare no conflicts to declare.

Data Availability Statement

The data that support the findings of this study are available from the corresponding author upon reasonable request.

Keywords

biodegradable, elastic scaffold, embolic agent, nanofibers, transcatheter arterial embolization

Received: December 25, 2023
Revised: January 22, 2024
Published online:

[1] L. M. Monsignore, S. Scarpelini, J. S. Santos, D. G. Abud, *Diagn. Interv. Radiol.* **2011**, *18*, 403.
[2] A. Poursaid, M. M. Jensen, E. Huo, H. Ghandehari, *J. Controlled Release* **2016**, *240*, 414.
[3] T. Yonemitsu, N. Kawai, M. Sato, T. Sonomura, I. Takasaka, M. Nakai, H. Minamiguchi, S. Sahara, Y. Iwasaki, T. Naka, M. Shinozaki, *Cardiovasc. Interv. Radiol.* **2010**, *33*, 1192.
[4] M. Bendszus, R. Klein, R. Burger, M. Warmuth-Metz, E. Hofmann, L. Solymosi, *Am. J. Neuroradiol.* **2000**, *21*, 255.
[5] J. Zhao, H. Lin, R. Summers, M. Yang, B. G. Cousins, J. Tsui, *Angiology* **2017**, *69*, 17.
[6] Y. Zhang, H. Gao, H. Wang, Z. Xu, X. Chen, B. Liu, Y. Shi, Y. Lu, L. Wen, Y. Li, Z. Li, Y. Men, X. Feng, W. Liu, *Adv. Funct. Mater.* **2018**, *28*, 1705962.
[7] I. Altun, J. Hu, H. Albadawi, Z. Zhang, M. A. Salomao, J. L. Mayer, L. Jamal, R. Oklu, *Adv. Mater.* **2020**, *32*, 2005603.
[8] B. Liu, Z. Xu, H. Gao, C. Fan, G. Ma, D. Zhang, M. Xiao, B. Zhang, Y. Yang, C. Cui, T. Wu, X. Feng, W. Liu, *Adv. Funct. Mater.* **2020**, *30*, 1910197.
[9] G. Go, H. W. Song, M. Nan, J. Lee, S. Kim, J. O. Park, E. Choi, *Adv. Funct. Mater.* **2023**, *33*, 2305205.
[10] Z. Zheng, H. Zhang, K. Qian, L. Li, D. Shi, R. Zhang, L. Li, H. Yu, C. Zheng, S. Xie, Y. Zhao, X. Yang, *Biomaterials* **2023**, *302*, 122324.
[11] M. Liu, Y. Wang, Y. Chen, L. Li, Y. Sun, Y. Li, Y. Yuan, P. Lu, W. Zhang, P. Pang, X. Peng, H. Shan, *Adv. Funct. Mater.* **2023**, *33*, 2305153.
[12] Q. Wang, Y. He, M. Shen, L. Huang, L. Ding, J. Hu, Y. Dong, H. Fu, Q. Wang, Y. Sun, L. Zhang, J. Cao, Y. Duan, *Adv. Funct. Mater.* **2021**, *31*, 2011170.
[13] J. Hu, H. Albadawi, B. W. Chong, A. R. Deipolyi, R. A. Sheth, A. Khademhosseini, R. Oklu, *Adv. Mater.* **2019**, *31*, 1901071.
[14] G. Ko, J. W. Choi, N. Lee, D. Kim, T. Hyeon, H.-C. Kim, *Biomaterials* **2022**, *287*, 121634.
[15] X. Mo, M. Shafiq, B. Sun, Y. Morsi, H. El-Hamshary, M. El-Newehy, M. Liu, Z. Yuan, Y. Chen, P. Cai, W. Guo, Y. Shen, J. Cui, X. Yu, *Front. Biosci. - Landmark* **2023**, *28*, 66.
[16] B. Sun, Y. Z. Long, H. D. Zhang, M. M. Li, J. L. Duvail, X. Y. Jiang, H. L. Yin, *Prog. Polym. Sci.* **2014**, *39*, 862.
[17] W. Chen, S. Chen, Y. Morsi, H. El-Hamshary, M. El-Newhy, C. Fan, X. Mo, *ACS Appl. Mater. Interfaces* **2016**, *8*, 24415.
[18] J. Zhang, L. Chen, J. Wang, Y. Lei, Y. Huang, J. Xu, N. Hu, W. Huang, W. Cui, X. Luo, *Adv. Funct. Mater.* **2022**, *33*, 2211237.
[19] X. Xie, D. Li, Y. Chen, Y. Shen, F. Yu, W. Wang, Z. Yuan, Y. Morsi, J. Wu, X. Mo, *Adv. Healthcare Mater.* **2021**, *10*, 2100918.
[20] L. Wang, Y. Qiu, Y. Guo, Y. Si, L. Liu, J. Cao, J. Yu, X. Li, Q. Zhang, B. Ding, *Nano Lett.* **2019**, *19*, 9112.
[21] C. Liu, K. Peng, Y. Wu, F. Fu, *Smart Med.* **2023**, *2*, 20230024.
[22] Y. Huang, X. Zhao, Z. Zhang, Y. Liang, Z. Yin, B. Chen, L. Bai, Y. Han, B. Guo, *Chem. Mater.* **2020**, *32*, 6595.
[23] Z. Zhang, H. Albadawi, R. J. Fowl, J. L. Mayer, B. W. Chong, R. Oklu, *Adv. Mater.* **2023**, *35*, 2305868.
[24] H. Ishikawa, H. Ohbe, N. Omachi, K. Morita, H. Yasunaga, *Radiology* **2021**, *298*, 673.
[25] J. Li, X. Yu, X. Shi, M. Shen, *Prog. Mater. Sci.* **2022**, *124*, 100871.
[26] J. Cheng, S. Feng, S. Han, X. Zhang, Y. Chen, X. Zhou, R. Wang, X. Li, H. Hu, J. Zhang, *ACS Nano* **2016**, *10*, 9957.
[27] B. Feng, H. Tu, H. Yuan, H. Peng, Y. Zhang, *Biomacromolecules* **2012**, *13*, 3917.
[28] K. M. Schelkle, C. Schmid, K. Yserentant, M. Bender, I. Wacker, M. Petzoldt, M. Hamburger, D. P. Herten, R. Wombacher, R. R. Schröder, U. H. F. Bunz, *Angew. Chem., Int. Ed.* **2017**, *56*, 4724.
[29] F. Zhou, L. Chen, Q. An, L. Chen, Y. Wen, F. Fang, W. Zhu, T. Yi, *Sci. Rep.* **2016**, *6*, 32145.
[30] Y. Huang, X. Zhao, C. Wang, J. Chen, Y. Liang, Z. Li, Y. Han, B. Guo, *Chem. Eng. J.* **2022**, *427*, 131977.
[31] Y. Luo, Y. Ma, Z. Chen, Y. Gao, Y. Zhou, X. Liu, X. Liu, X. Gao, Z. Li, C. Liu, H. L. Leo, H. Yu, Q. Guo, *Adv. Healthcare Mater.* **2022**, *11*, 2102281.
[32] R. Zheng, D. Song, Y. Ding, B. Sun, C. Lu, X. Mo, H. Xu, Y. Liu, J. Wu, *Front. Bioeng. Biotechnol.* **2023**, *11*, 1128762.
[33] W. Chen, Y. Xu, Y. Li, L. Jia, X. Mo, G. Jiang, G. Zhou, *Chem. Eng. J.* **2020**, *382*, 122986.
[34] P. Cai, C. Li, Y. Ding, H. Lu, X. Yu, J. Cui, F. Yu, H. Wang, J. Wu, M. El-Newehy, M. M. Abdulhameed, L. Song, X. Mo, B. Sun, *ACS Appl. Mater. Interfaces* **2023**, *15*, 54280.
[35] Y. Ding, W. Zhang, B. Sun, X. Mo, J. Wu, *J. Biomed. Mater. Res., Part A* **2022**, *110*, 1824.
[36] X. Ma, C. Wang, W. Yuan, X. Xie, Y. Song, *ACS Appl. Mater. Interfaces* **2021**, *3*, 6586.
[37] X. Wang, J. Zhu, B. Sun, Q. Jin, H. Li, C. Xia, H. Wang, X. Mo, J. Wu, *J. Biomed. Mater. Res., Part B* **2020**, *109*, 201.
[38] Y. Si, L. Wang, X. Wang, N. Tang, J. Yu, B. Ding, *Adv. Mater.* **2017**, *29*, 1700339.
[39] W. Guo, B. Zhao, M. Shafiq, X. Yu, Y. Shen, J. Cui, Y. Chen, P. Cai, Z. Yuan, M. El-Newehy, H. El-Hamshary, Y. Morsi, B. Sun, J. Pan, X. Mo, *Regen. Biomater.* **2023**, *10*, rbad019.
[40] K. Zhang, X. Bai, Z. Yuan, X. Cao, X. Jiao, Y. Li, Y. Qin, Y. Wen, X. Zhang, *Biomaterials* **2019**, *204*, 70.
[41] K. Quan, G. Li, L. Tao, Q. Xie, Q. Yuan, X. Wang, *ACS Appl. Mater. Interfaces* **2016**, *8*, 7666.
[42] L. Wang, Y. Zhong, C. Qian, D. Yang, J. Nie, G. Ma, *Acta Biomater.* **2020**, *114*, 193.
[43] H. Kuang, Y. Wang, Y. Shi, W. Yao, X. He, X. Liu, X. Mo, S. Lu, P. Zhang, *Biomaterials* **2020**, *259*, 120288.
[44] L. Fan, M. Duan, Z. Xie, K. Pan, X. Wang, X. Sun, Q. Wang, W. Rao, J. Liu, *Small* **2019**, *16*, 1903421.